Available online at www.eccomasproceedia.org
Eccomas Proceedia SMART (2023) 1601-1610

ECCOMAS
Proceedia

X ECCOMAS Thematic Conference on Smart Structures and Materials
SMART 2023
D.A. Saravanos, A. Benjeddou, N. Chrysochoidis and T. Theodosiou (Eds)

PROGRAMMING SHAPE MORPHING IN METAMATERIALS

Fanziska Wenz[1], Tobias Lichti[2], Angela Schwarz[3], Alexander Leichner[2], Heiko Andrae[2], Christof Huebner[3] and Christoph Eberl[1]

[1]Fraunhofer Institute for Mechanics of Materials (IWM)
79108 Freiburg, Germany
E-mail: franziska.wenz@iwm.fraunhofer.de, chris.eberl@iwm.fraunhofer.de
[2]Fraunhofer Institute for Industrial Mathematics (ITWM)
67663 Kaiserslautern, Germany
[3]Fraunhofer Institute for Chemical Technology (ICT)
76327 Pfinztal, Germany

Abstract. The internal structuring of materials on a mesoscale, e.g., µm-cm enables to design almost arbitrary effective physical properties into so called metamaterials. Moreover, programmable materials can be useful in application where conflicting conditions to the shape of the material exist (e.g., wings, personalized tools). They use a stimuli-excited change in the meso-structure to manipulate macroscopic properties in a controlled manner. The meso-structure is no longer static, but responsive to stimuli. The property changes can be either continuous, as a designed non-linear elastic behavior (processing a function), or abrupt (if-then-else condition). Such a logical behavior is implemented into unit cells to control the local Poisson's Ratio as well as the stiffness. These properties are related to geometrical parameters (angles, beam thicknesses) of unit cells that can be varied over a material's volume. The combination of the local unit cell logic and the global parameter distribution leads to a specific shape morphing behavior. Multiscale models and mathematical optimization methods enable us to compute optimal unit cell parameters for large cell arrays. Several unit cells created by different manufacturing methods (3D-printing, foil stacking) will be shown. The designed shape morphing behavior will be presented based on simulations as well as with physical demonstrators.

Key words: programmable materials, metamaterial, shape morphing, optimization, origami

1 INTRODUCTION

The internal structuring of materials on a mesoscale, e.g., µm-cm enables the design of effective mechanical properties [1]. In metamaterials even unexpected behavior such as auxeticity (negative Poisson's Ratio (PR)) is made possible by a proper design of their building blocks (unit cells) [2, 3, 4, 5]. Moreover, grading geometrical parameters of the unit cells over a material's volume allows for a local variation in stiffness and PR. The shape to which a material adapts when subjected to a mechanical load can be controlled by varying the distribution of these parameters. Such a shape matching was shown for different unit cells, e.g., honeycombs [6, 7],

Peer-review under responsibility of the organizing committee of SMART 2023.
doi: 10.7712/150123.9932.450753

star-shaped geometries [8, 9] or origami/kirigami foldings/cuttings [10, 11, 12]. Nevertheless, controlling the process of *how* a shape deforms requires considering non-linear base material behavior as well as the change in the geometry of the unit cell. For that reason, we describe this change in the meso-structure and the properties, respectively, by programming elements as processing functions and if-then-else conditions. The global material behavior is obtained by combining unit cells with different programs realized by adjusted geometrical parameters. The first part of the paper shows the different unit cells used to program shape morphing. Thereafter, the design of an optimized shape and its experimental validation is presented. Here, the use of multiscale models and mathematical optimization methods is introduced as well as the possibility of manufacturing large cell arrays based on foil stacking. Additionally, designs for controlling the complete morphing process, by varying multiple geometrical parameters simultaneously, will be shown. Finally, the combination of the different aspects, the possibility to use other triggers, and the potential of programmable shape morphing materials will be discussed.

2 UNIT CELLS

Figure 1 shows three types of unit cells and their geometrical parameters to achieve positive as well as negative PRs. Figure 1a and d are well known from literature: the PR of a hexagonal cell changes with its angle α ([6, 7]). For $\alpha > 90°$ the unit cell is a honeycomb with a positive PR (see figure 1a) and for $\alpha < 90°$ the shape is a bow-tie with negative PR (see figure 1d).
Going to folded structures, we can find similar behavior, but need two different parameters to obtain positive and negative PRs [13]. In Figure 1b the (positive) PR is controlled by the parameter V^* while $V = 0$ and in figure 1e the (negative) PR is adapted by the parameter V while $V^* = 0$. Both cells can be built by stacking of structured foils with different heights. The parameter h_2 describes the difference in height of two layers. The PR and stiffness are not constant but a function of strain. Additionally, the behavior can be described by a if-then-else condition. The stretching of the lower layer leads to an increase in the stiffness. The strain at which this change occurs depends on h_2.

The last cell can have both a positive or negative PR depending on the compression state (figure 1c and f) [14]. Hinges allow the beams to rotate during compression and α changes until the rotation is stopped by the blocks. The stiffness of the hinges is controlled by their thickness t_2 and the angle β determines the compressive strain where the stiffness suddenly increases. The behavior can be expressed as if-then-else condition (see equation (1)).

$$\textbf{if } \alpha(\varepsilon) > \beta \textbf{ then } \nu = f_1(\alpha)\ ,\ E = f_2(\alpha, t_2) \textbf{ else } \nu \approx 0\ ,\ E = f_3 \tag{1}$$

The condition can be set up by choosing β and the non-linear functions in the statements can be adjusted by α and t_2.

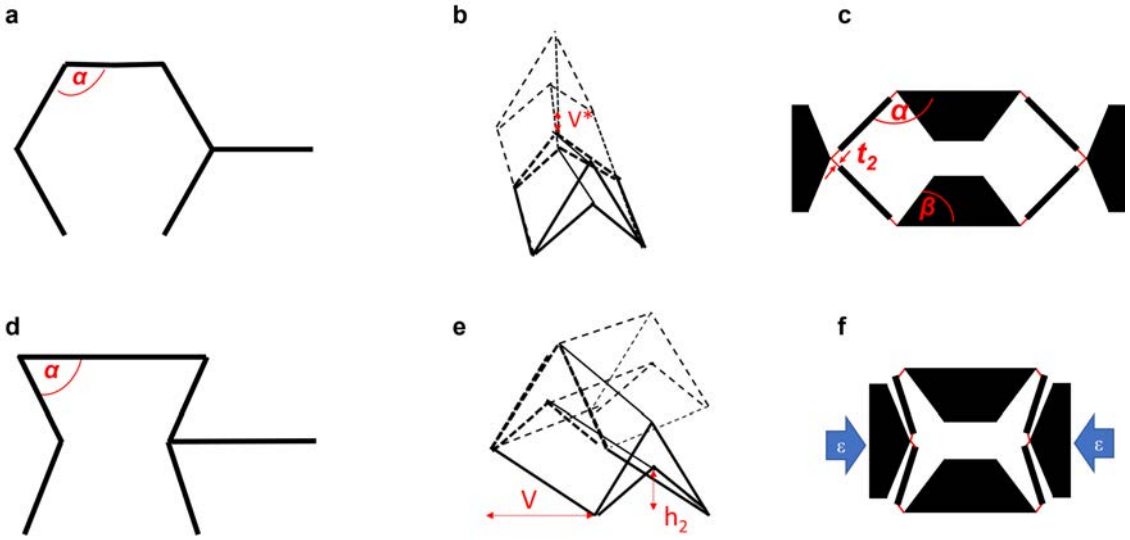

Figure 1: Different unit cells and geometrical parameters to control the PR for shape morphing: a honeycomb cell (positive PR) , b Eggbox folding (positive PR) [13], c adapted honeycomb (positive PR) [14], d bow-tie cell (negative PR), e Miura-Ori folding (negative PR) [13], f compressed adapted honeycomb (negative PR)

3 MATERIAL BEHAVIOR

To illustrate possible material behavior various unit cells were combined in 2D- as well as 3D-arrays. The geometrical parameters in the cells are variable but the size of the unit cells is constant so that a proper assembly of the cells is ensured. Additionally, the coordinates of nodes or faces that are shared by several cells were averaged to obtain a connected material. Two examples of such materials will be presented. One shows the control of a simple shape change and the possibility to manufacture a large number of unit cells and to calculate the necessary parameter distributions for a target shape. The second one allows for controlling complex shape morphing but still poses challenges to manufacturing and simulation techniques.

3.1 Targeted Shape Morphing

The unit cells presented in figure 1b and e can be produced by the stacking of foils. Using flexible base materials in combination with deep-drawing allows to generate structures with a variable meso-structure that can be largely deformed. For that reason, a manufacturing method for stacks of thermoplastic polyurethane (TPU) foils was established in [15]. The single layers can be structured by using individual, 3D-printed molds during the thermoforming process. Parts of multiple layers built the unit cells in the material. With the help of this technique, hundreds of individual unit cells can be produced in a scalable manner. To create a desired complex target shape within such layers or stacks, the parameter V, V^*, and h_2 have to be varied in all directions in the material's volume. Adequate models are necessary for finding optimal

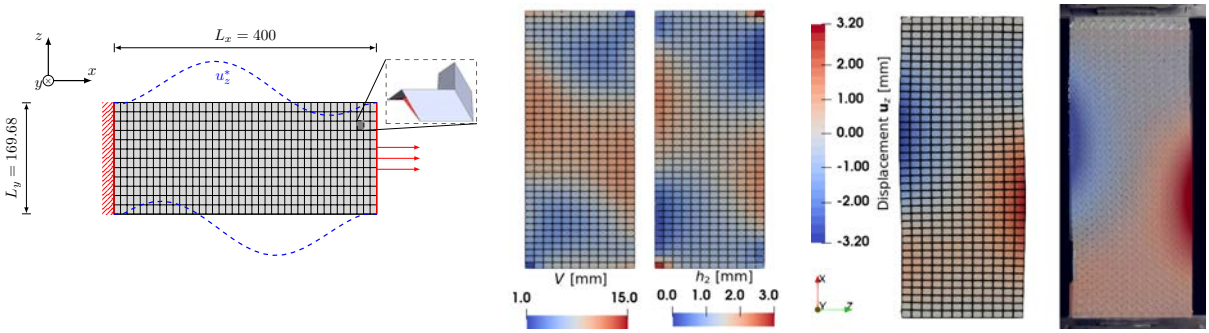

Figure 2: Left: Multiscale optimization problem: Array of unit cells parameterized by V and h_2 and a target shape u_z, middle: optimal parameter distributions, right: comparison of the displacement calculated by the surrogate model and from experiments. Adapted from [15, 17].

parameter distributions by mathematical optimization. They allow to replace every unit cell with a solid hexagonal element with equivalent macroscopic behavior. Therefore, a database out of homogenized stresses of single unit cells for different load cases was precomputed. For the modeling of the base material (TPU) a Mooney-Rivlin model with the parameters $C_{10} = 0\,\text{MPa},\ C_{01} = 6.29\,\text{MPa}, D = 10^{-3}\,\frac{1}{\text{MPa}}$ obtained from experiments and a shell thickness $d = 0.4$ mm were used. The data points were not only sampled in the strain space but also the design space (here variations of V, h_2). The database

$$\widehat{S}(V, h_2, \widehat{C}) \approx \widehat{D}(V, h_2, \widehat{C}) \tag{2}$$

maps the macroscopic strain ($\widehat{C}$, right Cauchy-Green strain tensor) and the design parameters (V, h_2) to homogenized stress ($\widehat{S}$, second Piola Kirchhoff stress tensor). For the resulting surrogate model tensor decomposition and spline interpolation as described in [16] were used. By calculating the derivative of the interpolation function, the derivatives w.r.t. strain and design parameters are obtained. More details on the modeling, the optimization procedure, and examples for additional unit cells can be found in [17].
First an unsymmetrical target deformation u_z^* was defined (see figure 2 left) and the parameter distributions for V and h_2 were calculated by using the surrogate model in combination with mathematical optimization. Figure 2, middle shows the distribution of V and h_2 in a plane. Two foil layers of different heights were manufactured with such a parameter distribution and a tensile test was performed to validate the models. Local displacements were analyzed by using digital image correlation. On the right figure, the displacements of the experiments as well as of simulations are displayed at 5% strain. They show a good qualitative agreement, but the magnitude of the displacements are approximately 10% larger in the experiments. Yet, the predefined target shape was achieved. The difference can originate from the fact that in the manufactured sample micro-fluctuations occur, leading to slightly larger displacements on the boundaries.

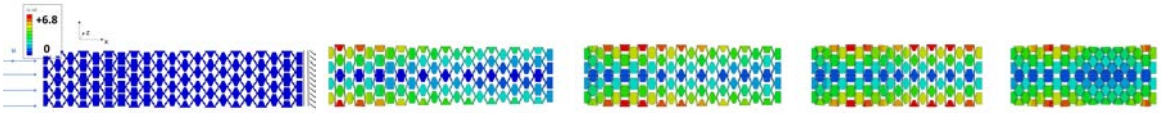

Figure 3: FE-simulations of a material with a gradient in the geometrical parameters t_2 and β. Boundary conditions are displayed in the left image. Local deformations (displacement in y-direction) and the deformed shape are shown for an increasing load (from left to right).

3.2 Complex Shape Morphing

Moreover, using more complex unit cells enables not only the control of the target shape but also of the morphing behavior. To illustrate the possibilities two parameters (t_2 and β) were varied in an array built of the unit cells shown in figure 1c. For this purpose, a script was created that generates the geometries for a given set of parameters in the software *Abaqus 2021*. Linear elastic material behavior ($E = 1000$, $\nu = 0$) was assumed for the base material and a hard contact without friction between the contact surfaces was modeled. The geometries were meshed with C3D8 hexahedral elements using adaptive mesh control. Finite element (FE) simulations were performed on structures of 2x10 cells that were mirrored on the xz-plane. They were compressed in y-direction (displacement on the left side and y-symmetry on the right side of the material) as shown in figure 3 left. Different magnitudes of displacements (u_x) were applied and the corresponding deformation of the structure in the transverse direction was investigated. Figure 3 shows the local displacements of the structure in the y-directions for increasing load from left to right.

To compare the behavior of different parameter variations, coordinates of the upper edge of the material at different displacement amplitudes were evaluated. Figure 4 shows the distribution of the parameters t_2 and β and the coordinates (lines) of the corresponding materials' deformations. In figure 4a both geometrical parameters are constant. The deformation of the surface under compression is at first increasing (positive PR) and later decreasing (negative PR). Additionally, the length of the material is decreasing (shorter lines). All cells show the same behavior, only some tipping due to numerical and mechanical instabilities occurs. In the second example (figure 4b) t_2 is constant but β varies according to the presented parameter distribution. The start of the deformation looks similar to figure 4a but the final shape is not a straight surface but a curved one. The beginning of the deformation is only controlled by t_2 and α but the stopping point in the deformation and consequently the final shape is determined by the distribution of β. On the contrary to that, the parameter t_2 is varied and β is constant in figure 4c. In consequence, the softer part (left side) of the material starts to deform at first and a bulge is moving through the material due to the gradient in the stiffness. At the different displacements shown in the plot, some of the cells are in a configuration with positive PR and others with negative PR depending on the local strain. Due to changes in the configurations, the shape is morphing. Nevertheless, the final shape is straight due to the uniform contact block geometries. Finally, a variation of both parameters is presented in figure 4d. Here, we find a mixture of examples b and c. At the start, the behavior originating from the gradient in t_2 is

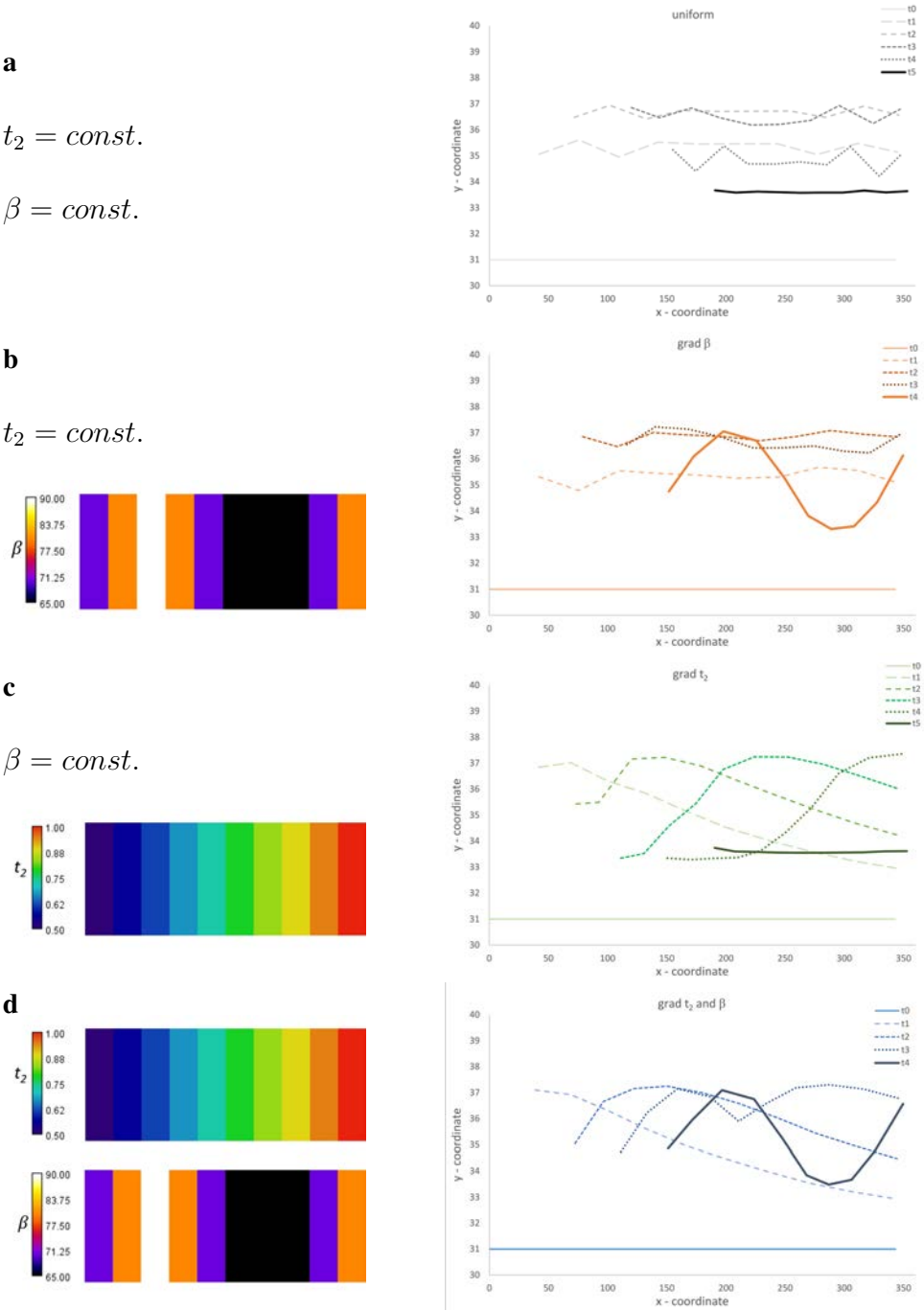

Figure 4: Shape of the material's surface (x- and y-coordinates) at increasing compressive strain ($u_x(t_0) < u_x(t_1) < u_x(t_2) < u_x(t_3) < u_x(t_4)$) for different parameter distributions (t_2, β). a: β and t_2 are fixed values, uniform material, b: β is varied over the x-coordinate, final shape is non-uniform, c: t_2 is varied over the x-coordinate, different shapes during morphing, d: β and t_2 are varied over the x-coordinate, shape morphing and non-uniform final shape.

dominant. Later, some cells are going into contact, and the shape also depends on β. In the end, the final shape is determined by the distribution of β and independent on t_2. The deformation of such a structure is shown in figure 3, where the subfigures correspond to the five lines in the 4d.

4 DISCUSSION

Programming material behavior not only requires controlling single unit cells but also the combination of them. The design of different target shapes by choosing parameter distributions was transferred from honeycomb structures [7, 6] to scalable unit cells. The ability to create large arrays in combination with optimization methods allows for designing individually adjusted shape morphing materials. The approach is not limited to the cell design used for the presented example but also for other foldable unit cells such as shown in figure 1b. Therefore, the database in equation (2) has to be extended to track additional design parameters. Additionally, variations in manufactured cells with respect to the ideal geometry (e.g., non-uniform foil thickness) should be further analyzed and taken into account in the design process to reduce the difference between simulations and measurements.
More complex shape morphing behavior was analyzed by FE-simulations. Nevertheless, a 3D-printed demonstrator of a similar design is presented in [14]. The gradients in the different parameters are difficult to realize in a scalable manufacturing process. Yet, e.g., combining foils with varying thicknesses in combination with graded structures could be a first approach. Additionally, bringing such a structure into the database poses challenges. In the strain space, many instable states exist which makes the precomputing complicated and history-dependent. Nevertheless, some approaches to simulate multi-stable structures are presented in [18, 19].

5 OUTLOOK

Unit cells as well as methods to combine them for the design of shape morphing have been presented. Not only the final shapes but also different ways how the shape can be achieved have been shown. If the whole spectrum of programmable materials is used, bistable elements can additionally be introduced, which help to memorize a shape [20, 21]. Moreover, temperature can be implemented as a trigger for restoring the memory elements [14], or to create a targeted shape change e.g., by controlling the coefficient of thermal expansion [22]. The presented database approach can be extended to consider the latter. This also enables to simulate combinations of the different programming elements that can fulfill more complicated target functions. Such behavior has the potential to replace systems (e.g., hinges, actuation by electrical motors), improve applications (e.g., personalized tools, seats), or create novel functionalities (storing energy from deformations, adapting to improve air resistance).

REFERENCES

[1] M. Kadic, G. Milton, M. Hecke, and M. Wegener, "3d metamaterials," *Nature Reviews Physics*, p. 1, 01 2019. [Online]. Available: https://www.nature.com/articles/s42254-018-0018-y

[2] H. A. Kolken and A. A. Zadpoor, "Auxetic mechanical metamaterials," *RSC Adv.*, vol. 7, pp. 5111–5129, 2017. [Online]. Available: http://dx.doi.org/10.1039/C6RA27333E

[3] R. Almgren, "An isotropic three-dimensional structure with poisson's ratio= -1," *Journal of elasticity*, vol. 15, pp. 427–430, 1985.

[4] R. Lakes and K. W. Wojciechowski, "Negative compressibility, negative poisson's ratio, and stability," *physica status solidi (b)*, vol. 245, no. 3, pp. 545–551, 2008. [Online]. Available: https://onlinelibrary.wiley.com/doi/abs/10.1002/pssb.200777708

[5] J. N. Grima, P.-S. Farrugia, R. Gatt, and D. Attard, "On the auxetic properties of rotating rhombi and parallelograms: A preliminary investigation," *physica status solidi (b)*, vol. 245, no. 3, pp. 521–529, 2008. [Online]. Available: https://onlinelibrary.wiley.com/doi/abs/10.1002/pssb.200777705

[6] Y. Han and W. Lu, "Evolutionary design of nonuniform cellular structures with optimized poisson's ratio distribution," *Materials and Design*, vol. 141, pp. 384 – 394, 2018. [Online]. Available: https://doi.org/10.1016/j.matdes.2017.12.047

[7] M. Mirzaali, S. Janbaz, and M. Strano, "Shape-matching soft mechanical metamaterials," *Sci Rep*, vol. 8, 2018.

[8] J. Martínez, M. Skouras, C. Schumacher, S. Hornus, S. Lefebvre, and B. Thomaszewski, "Star-shaped metrics for mechanical metamaterial design," vol. 38, no. 4, jul 2019. [Online]. Available: https://doi.org/10.1145/3306346.3322989

[9] K. K. Dudek, J. A. I. Martínez, G. Ulliac, and M. Kadic, "Micro-scale auxetic hierarchical mechanical metamaterials for shape morphing," *Advanced Materials*, vol. 34, no. 14, p. 2110115, 2022. [Online]. Available: https://onlinelibrary.wiley.com/doi/abs/10.1002/adma.202110115

[10] P. Celli, C. McMahan, B. Ramirez, A. Bauhofer, C. Naify, D. Hofmann, B. Audoly, and C. Daraio, "Shape-morphing architected sheets with non-periodic cut patterns," *Soft Matter Communication*, 2018. [Online]. Available: https://pubs.rsc.org/en/content/articlelanding/2018/sm/c8sm02082e

[11] L. Dudte, E. Vouga, T. Tachi, and L. Mahadevan, "Programming curvature using origami tessellations," *Nature Materials*, vol. 15, 01 2016.

[12] T. Gao, E. Siéfert, A. DeSimone, and B. Roman, "Shape programming: Shape programming by modulating actuation over hierarchical length scales (adv. mater. 47/2020)," *Advanced Materials*, vol. 32, no. 47, p. 2070349, 2020. [Online]. Available: https://onlinelibrary.wiley.com/doi/abs/10.1002/adma.202070349

[13] M. Schenk and S. Guest, "Origami folding: A structural engineering approach," 07 2010.

[14] F. Wenz, I. Schmidt, A. Leichner, T. Lichti, S. Baumann, H. Andrae, and C. Eberl, "Designing shape morphing behavior through local programming of mechanical metamaterials," *Advanced Materials*, vol. 33, no. 37, p. 2008617, 2021. [Online]. Available: https://onlinelibrary.wiley.com/doi/abs/10.1002/adma.202008617

[15] A. Schwarz, T. Lichti, F. Wenz, B. M. Scheuring, C. Hübner, C. Eberl, and P. Elsner, "Development of a scalable fabrication concept for sustainable, programmable shape-morphing metamaterials," *Advanced Engineering Materials*, vol. 24, no. 11, p. 2200386, 2022. [Online]. Available: https://onlinelibrary.wiley.com/doi/abs/10.1002/adem.202200386

[16] J. Yvonnet, E. Monteiro, and Q.-C. He, "Computational homogenization method and reduced database model for hyperelastic heterogeneous structures," *International Journal for Multiscale Computational Engineering*, vol. 11, 01 2013.

[17] T. Lichti, A. Leichner, H. Andrä, R. Müller, F. Wenz, C. Eberl, A. Schwarz, and C. Hübner, "Optimal design of shape changing mechanical metamaterials at finite strains," *International Journal of Solids and Structures*, p. 111769, 2022. [Online]. Available: https://www.sciencedirect.com/science/article/pii/S0020768322002621

[18] R. Khajehtourian and D. Kochmann, "A continuum description of substrate-free dissipative reconfigurable metamaterials," *Journal of the Mechanics and Physics of Solids*, vol. 147, 11 2020. [Online]. Available: https://www.sciencedirect.com/science/article/pii/S0022509620304324

[19] Y. Li, "A method of designing a prescribed energy landscape for morphing structures," *International Journal of Solids and Structures*, vol. 242, p. 111500, 2022. [Online]. Available: https://www.sciencedirect.com/science/article/pii/S0020768322000609

[20] T. Chen, J. Panetta, M. Schnaubelt, and M. Pauly, "Bistable auxetic surface structures," *ACM Trans. Graph.*, vol. 40, no. 4, Jul. 2021. [Online]. Available: https://doi.org/10.1145/3450626.3459940

[21] M. F. Berwind, A. Kamas, and C. Eberl, "A hierarchical programmable mechanical metamaterial unit cell showing metastable shape memory," *Advanced Engineering Materials*, vol. 20, no. 11, p. 1800771, 2018. [Online]. Available: https://onlinelibrary.wiley.com/doi/abs/10.1002/adem.201800771

[22] H. Xu, A. Farag, and D. Pasini, “Routes to program thermal expansion in three-dimensional lattice metamaterials built from tetrahedral building blocks,” *Journal of the Mechanics and Physics of Solids*, vol. 117, pp. 54–87, 2018. [Online]. Available: https://www.sciencedirect.com/science/article/pii/S0022509618300437